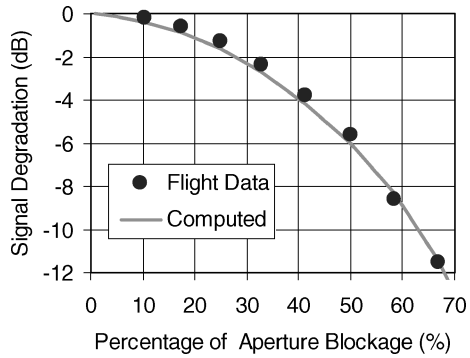

Fig. 6 Signal strength reduction as a function of percentage of ISS Ku-band antenna aperture blockage.

the signal strength decreases as the structure penetraties the antenna aperture projected cylinder. The gain reduction is mainly due to decreasing aperture area or effective antenna size and can be estimated based on the aperture blockage area, as shown in Fig. 6, derived from averaging the solar panel and radiator blockage results. Another factor causing gain reduction is the shift of the antenna main beam pattern (sum and difference patterns). However, it is not significant enough to impact the ISS antenna autotracking performance.

As shown in Figs. 2 and 3, the flight data reach a floor value of about −57 dBm. The simulation results actually decrease even further, depending on the size of the remaining unblocked aperture area. The signal strength increases after structure blockage of the antenna aperture projected cylinder ceases. The computed results, in general, predict a deeper null caused by the solar panel blockage. This is expected because the solar panel was modeled as a perfect conducting plate in the simulations. The actual solar array panel is a composite structure formed by closely spaced solar cells. The flight data indicate that the Ku band can withstand 4.6-dB degradation and still maintain the data flow. The GTD simulations indicate that a 4.6-dB degradation corresponds to about 40% aperture blockage. The ISS Ku-band communication link will be considered lost if more than 40% of the aperture projected cylinder is blocked by ISS structures.

Conclusions

The ISS Ku-band antenna model for communication coverage analysis[1] is updated and validated using recently obtained flight data. The flight data indicate the ISS Ku-band link can sustain 4.6-dB degradation from structure blockage. The updated antenna model for the ISS Ku-band reflector antenna, based on the flight data and GTD simulations, allows up to 40% structure blockage of the antenna aperture before declaring Ku-band communication outages. The communication coverage based on the updated antenna model reflects the actual Ku-band link margin and antenna performance. A better match in the communication coverage is achieved between computer simulations and actual measurements.

References

[1]Hwu, S. U., Lu, B. P., Johnson, L. A., Fournet, J. S., Panneton, R. J., and Arndt, G. D., "Scattering Properties of Solar Panels for Antenna Pattern Analysis," *Proceedings of IEEE International Antennas and Propagation Symposium & URSI Radio Science Meeting*, Inst. of Electrical and Electronics Engineers, Piscataway, NJ, 1994, pp. 266–269.

[2]Lewis, R. L., and Newell, A. C., "Efficient and Accurate Method for Calculating and Representing Power Density in the Near Zone of Microwave Antennas," *IEEE Transactions on Antennas and Propagation*, Vol. 36, No. 6, 1988, pp. 890–901.

[3]Kouyoumijian, R. G., and Pathak, P. H., "A Uniform Geometrical Theory of Diffraction for an Edge in a Perfectly Conducting Surface," *Proceedings of IEEE*, Vol. 62, No. 11, 1974, pp. 1448–1461.

[4]Marhefka, R. J., and Silvestro, J. W., "Near Zone—Basic Scattering Code User's Manual with Space Station Applications," NASA CR-181944, Dec. 1989.

N. Gatsonis
Associate Editor

Optimal Control of Tethered Planetary Capture Missions

Paul Williams*
Royal Melbourne Institute of Technology, Melbourne, Victoria 3001, Australia

Nomenclature

A	=	tether cross-sectional area, m^2
a	=	semimajor axis of orbit, m
e	=	orbit eccentricity
F	=	factor of safety for tether material, 1.5
f	=	orbit true anomaly of the tether system center of mass, rad
g	=	gravitational acceleration at Earth sea level, 9.81 m/s^2
I_{sp}	=	specific impulse of chemical propellant, s
L	=	tether reference length, m
l	=	tether length, m
m	=	total system mass, $m_1 + m_2 + m_t$, kg
m_t	=	deployed tether mass, ρAl, kg
m_1	=	mass of main spacecraft, kg
m_2	=	mass of payload, kg
m^*	=	reduced system mass, kg
R	=	orbit radius to the system center of mass, m
R_p	=	periapsis radius of approach hyperbolic orbit, m
T	=	tether control tension, N
u	=	nondimensional control tension, $T/[m_1 \dot{f}^2 L(m_2 + m_t)/m]$
v_∞	=	hyperbolic approach velocity, m/s
θ	=	in-plane tether libration angle, rad
Λ	=	nondimensional tether length, l/L
μ	=	gravitational constant of central planet, km^3/s^2
ρ	=	tether mass density, kg/m^3
σ_{ut}	=	ultimate tensile strength of tether material, N/m^2

Superscripts

$\cdot$	=	differentiation with respect to time, d( )/dt
$'$	=	differentiation with respect to orbit true anomaly, d( )/df

Introduction

TETHERED spacecraft have been proposed for a wide variety of advanced space applications, both in the vicinity of the Earth and in interplanetary missions.[1] A new application of tethers in interplanetary spaceflight, first mentioned by Longuski et al.,[2] has been further investigated by Williams et al.[3,4] In this application, called tethered planetary capture, a tethered payload is deployed from a mother spacecraft while the system is on a hyperbolic flyby trajectory of a target planet. The basic maneuver is depicted in Fig. 1, which shows the following: 1) The payload is deployed via a tether in a hyperbolic approach orbit and made to spin or swing in the positive direction indicted in Fig. 1. 2) The payload is released from the tether at an appropriate moment so that it is captured into an elliptical orbit. 3) The main spacecraft gains an additional boost and is sent on a new escape trajectory. By suitable selection of system parameters, such as tether length and spin rate, it is possible to achieve planetary capture without expending any chemical propellant.

The dynamics of the tethered planetary capture maneuver, as well as preliminary control schemes were presented by Williams et al.[3,4]

Received 10 September 2003; revision received 13 December 2003; accepted for publication 15 December 2003.

*Ph.D. Candidate, Department of Aerospace Engineering, G.P.O. Box 2476V; tethers@hotmail.com. Student Member AIAA.

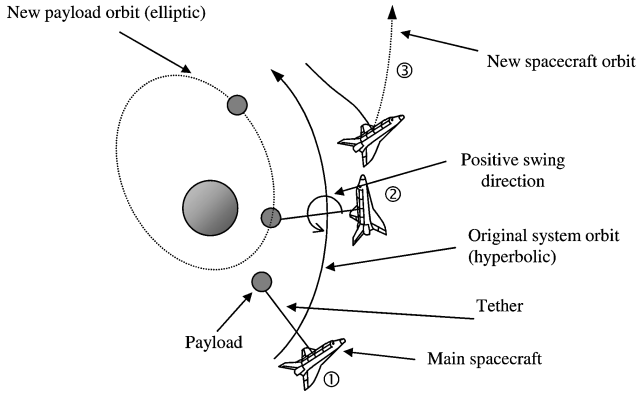

Fig. 1 Tethered planetary capture concept.

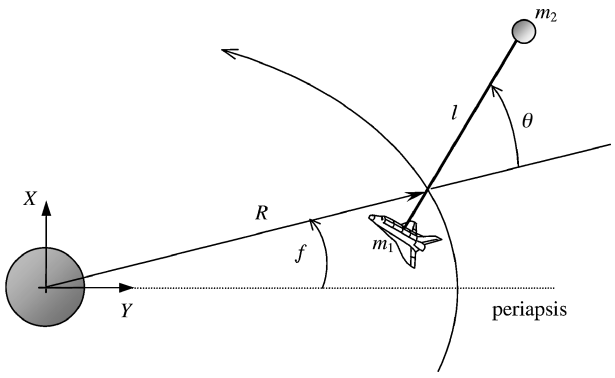

Fig. 2 Simplified tether system model.

Significant mass savings are possible at each of the major planets in the solar system by employing tethers to perform the planetary capture maneuver compared to a conventional propellant rocket system. It has also been shown that it is possible to use the Coriolis forces generated by tether reeling to guide the system from an infeasible capture scenario to one where planetary capture can take place. By infeasible, it is meant that at no point during the flyby can the payload be released into an elliptical orbit. A control discretization method combined with simulated annealing was employed in Ref. 4, where the required reel rates for the tether deployer were found to be quite large, that is, 100–150 m/s. The focus of Refs. 3 and 4 is on optimal tether mass configurations, where the tether system is required to spin quite rapidly as it commences the hyperbolic flyby, rather than on the use of tether reeling. In this Note, optimal control methodology is used to obtain planetary capture trajectories at Venus and Jupiter. In these scenarios, the tether is initially nonspinning and tether reeling is used to control the length and rotation of the tether. A Chebyshev pseudospectral method is used to convert the continuous optimal control problem to a discrete nonlinear programming problem. This approach allows additional parameters such as the tether mass to be determined in a straightforward manner.

Equations of Motion

The tether system model is shown in Fig. 2. The mother spacecraft m_1 and the payload m_2 are modeled as point masses, whereas the tether is modeled as a uniform inextensible rod of variable length with mass density ρ and cross-sectional area A. The applied control force is assumed to be the nondimensional tether tension at the mother spacecraft u. The Lagrangian for the system is given by[4]

$$\mathcal{L} = \frac{1}{2}\left[\frac{m_1(m_2+m_t)}{m}\right]\dot{l}^2 + \tfrac{1}{2}m^*l^2(\dot{\theta}+\dot{f})^2 + \tfrac{1}{2}m(\dot{R}^2+R^2\dot{f}^2) + \frac{\mu m}{R} - \frac{\mu m^* l^1(1-3\cos^2\theta)}{(2R^3)} \tag{1}$$

where $m^* = (m_1 + m_t/2)(m_2 + m_t/2)/m - m_t/6$ is the reduced mass of the system. The equations of motion for the system center of mass, derived via Lagrange's equations based on Eq. (1), are coupled with the tether libration dynamics. However, numerical simulations show that the orbital perturbations are relatively weak for the hyperbolic orbits considered in this Note and are ignored. Hence, the coordinates R and f may be determined from astrodynamics as

$$R = \frac{a(1-e^2)}{(1+e\cos f)} \tag{2}$$

$$\dot{f} = (1+e\cos f)^2\sqrt{\frac{\mu}{(a[1-e^2])^3}} \tag{3}$$

Note that it is assumed that the tether system is within the target planet's sphere of influence, and perturbations from the sun and other planets are ignored. Under the aforementioned assumptions, the nondimensional equations of motion for the tether system are[4]

$$\theta'' = 2(\theta'+1)\left[\frac{e\sin f}{1+e\cos f} - \frac{m_1(m_2+m_t/2)}{mm^*}\frac{\Lambda'}{\Lambda}\right] - \frac{3}{1+e\cos f}\sin\theta\cos\theta \tag{4}$$

$$\Lambda'' = \frac{2e\sin f}{1+e\cos f}\Lambda' - \frac{(2m_1-m)m_t/2}{m_1(m_2+m_t)}\frac{\Lambda'^2}{\Lambda} + \left(\frac{m_2+m_t/2}{m_2+m_t}\right)\Lambda \times\left[(\theta'+1)^2 + \frac{1}{1+e\cos f}(3\cos^2\theta-1)\right] - u \tag{5}$$

Note that Eq. (5) models the change in tether length due to tension control, but does not model the inertia or friction of the reel system.

When the end masses are released from the tether, the orbit of each mass is determined by its instantaneous position and velocity vectors. For example, the eccentricity is the magnitude of the eccentricity vector, which can be calculated with the equation

$$\boldsymbol{e} = (1/\mu)\left(V_x^2 - \mu/R_x\right)\boldsymbol{R}_x - (1/\mu)(\boldsymbol{R}_x\cdot\boldsymbol{V}_x)\boldsymbol{V}_x \tag{6}$$

where

$$\boldsymbol{R}_x = \begin{Bmatrix} R\cos f + x\cos(f+\theta) \\ R\sin f + x\sin(f+\theta) \end{Bmatrix} \tag{7}$$

$$\boldsymbol{V}_x = \begin{Bmatrix} \dot{R}\cos f - R\dot{f}\sin f + \dot{x}\cos(f+\theta) - x(\dot{f}+\dot{\theta})\sin(f+\theta) \\ \dot{R}\sin f + R\dot{f}\cos f + \dot{x}\sin(f+\theta) + x(\dot{f}+\dot{\theta})\cos(f+\theta) \end{Bmatrix} \tag{8}$$

where $x = -(m_2+m_t/2)l/m$ for the main spacecraft and $x = (m_1+m_t/2)l/m$ for the payload.

The required propellant mass m_{prop} to transfer the payload from the incoming hyperbolic orbit to a parabolic orbit may be calculated from[2]

$$\Delta v = \sqrt{2\mu/r_p + v_\infty^2} - \sqrt{2\mu/r_p}$$

$$m_{\text{prop}} = m_2[\exp(\Delta v/I_{\text{sp}}g) - 1] \tag{9}$$

Optimal Control Problem

The objective of the planetary capture maneuver is to deploy a payload on a tether such that at some point during the hyperbolic flyby it can be released into a captured orbit ($e < 1$). It is also desirable from a practical point of view to minimize the amount of work done by the reel mechanism to reduce system power requirements. Furthermore, to provide an advantage over the use of chemical propellant, it is desirable to keep the mass of tether as low as possible. The work done by the reel mechanism is given by

$$W = T\dot{l} = [m_1(m_2+m_t)/m]u\dot{f}^2L(\Lambda' L\dot{f}) \tag{10}$$

The cost function selected for this problem is a linear combination of the reel work squared and tether mass:

$$\mathcal{J} = \frac{1}{2}\int_{t_0}^{t_f} \left[w_1 W^2 + w_2 m_t\right] \mathrm{d}f \tag{11}$$

where w_1 and w_2 are weighting coefficients. The square of the work done by the reel can be expected to be larger than the tether mass, and, hence, the weights are selected as $w_1 = 0.01$ and $w_2 = 0.1$. Other choices for the weights are possible, depending on the desired penalties on the respective quantities. Note that the tether mass in Eq. (11) is a function of the instantaneous tether length during the maneuver. The control problem is to find the nondimensional control tension $u(f)$ tether cross-sectional area A and the final time t_f that minimizes Eq. (11) subject to the constraints

$$e_2(t_f) \le 0.995 \tag{12}$$

$$u(f) \ge 0.001 \tag{13}$$

$$T(f) \le \sigma_{ut} A/F \tag{14}$$

together with the state equations (4) and (5), and the initial conditions

$$\{\theta, \theta', \Lambda, \Lambda'\}|_{t_0} = \{\theta_0, \theta_0', \Lambda_0, \Lambda_0'\} \tag{15}$$

The constraint given by Eq. (12) ensures that the payload at the release point t_f enters into a captured orbit. The final maximum allowable eccentricity, $e_2 = 0.995$ is selected to be sufficiently less than that required for a parabolic orbit, so that timing errors of several minutes for payload release are permissible. It is also chosen to be consistent with earlier work.[4] The constraint given by Eq. (13) ensures that the tether remains in tension, and the constraint given by Eq. (14) ensures that the design tension exceeds or is equal to the instantaneous tension during the maneuver. Note that the tension is not constant along a massive tether,[5] and the control tension is used as an approximation to the design tension in Eq. (14).

Several methods are available for the solution of optimal control problems, such as shooting,[6] gradient,[6] and continuation methods.[7] These methods are based on derivation of the necessary conditions for optimality by the use of the calculus of variations and are commonly referred to as indirect methods.[8] Indirect methods are often extremely difficult to solve unless good guesses for the states and adjoints are available. Alternatively, direct methods convert the original problem into a parameter optimization problem by a suitable discretization scheme.[9] Several methods have been proposed that differ in the way the state equations are approximated. Pseudospectral methods[10,11] have emerged as an efficient and reliable direct approach that are relatively simple to implement. A pseudospectral method is used in this Note because of its reliability[12] and because it requires a smaller number of optimization variables compared to other popular direct methods for similar accuracy.[11]

In this Note, the Chebyshev pseudospectral method is employed (see Ref. 11). The Chebyshev method was selected over the Legendre method (see Ref. 10) because the Chebyshev–Gauss–Lobatto (CGL) nodes are available in closed form. In this method, the state and control vectors are expanded with Nth degree global Lagrange interpolating polynomials based on the CGL points

$$\boldsymbol{x}_N(\tau) = \sum_{j=0}^{N} \hat{\boldsymbol{x}}_j \phi_j(\tau), \qquad \boldsymbol{u}_N(\tau) = \sum_{j=0}^{N} \hat{\boldsymbol{u}}_j \phi_j(\tau) \tag{16}$$

where $\hat{\boldsymbol{x}}_j, \hat{\boldsymbol{u}}_j$, $j = 0, \ldots, N$, are the coefficients of the interpolating polynomial. The coefficients are given by $\hat{\boldsymbol{x}}_j = \boldsymbol{x}_N(\tau_j)$, and $\hat{\boldsymbol{u}}_j = \boldsymbol{u}_N(\tau_j)$, where $\tau_j = -\cos(\pi j/N)$, $j = 0, \ldots, N$, are the CGL points and $\phi_j(\tau)$ are the Lagrange interpolating polynomials. The CGL points lie in the domain $\tau \in [-1, 1]$ and must be mapped to the physical domain, $f \in [t_0, t_f]$ by the linear transformation $f = \{(t_f - t_0)\tau + t_0 + t_f\}/2$.

Approximations to the state dynamics are obtained by direct differentiation of the approximating polynomial for the states in Eq. (16) and setting them to be equal to the state equations at the CGL points. Derivatives of the state vector at the CGL points may be related to the state vector at the CGL points by way of a differentiation matrix

$$\boldsymbol{x}_N'(f_k) = \frac{2}{t_f - t_0}\boldsymbol{x}_N'(\tau_k) = \frac{2}{t_f - t_0}\sum_{j=0}^{N} \hat{\boldsymbol{x}}_j \phi_j'(\tau_k) = \frac{2}{t_f - t_0}\sum_{j=0}^{N} \mathcal{D}_{kj}\hat{\boldsymbol{x}}_j \tag{17}$$

where the coefficients $\mathcal{D}_{kj}$ are entries of a $(N+1)\times(N+1)$ differentiation matrix $\mathcal{D}$

$$\mathcal{D} := [\mathcal{D}_{kj}]$$

$$= \begin{cases} (c_k)/c_j\left[(-1)^{j+k}\big/(\tau_k - \tau_j)\right], & j \ne k \\ -\tau_k\big/\left[2\left(1-\tau_k^2\right)\right], & 1 \le j = k \le N-1 \\ -(2N^2+1)/6, & j = k = 0 \\ (2N^2+1)/6, & j = k = N \end{cases} \tag{18}$$

with $c_j = 1$ for $1 \le j \le N-1$ and $c_j = 2$ for $j = 0$ and N. The integral cost function is approximated by the Clenshaw–Curtis quadrature rule

$$\int_{t_0}^{t_f} p(f)\,\mathrm{d}f = \frac{t_f - t_0}{2}\int_{-1}^{1} p(\tau)\,\mathrm{d}\tau \cong \frac{t_f - t_0}{2}\sum_{j=0}^{N} p(\tau_j) w_j \tag{19}$$

where N is even

$$w_j = \begin{cases} 1/(N^2-1), & j = 0, N \\ \dfrac{4}{N}\displaystyle\sum_{k=0}^{N/2}\frac{1}{\bar{c}_k}\frac{\cos(2\pi jk/N)}{1-4k^2}, & j = 1, \ldots, N-1 \end{cases} \tag{20}$$

with $\bar{c}_0 = \bar{c}_{N/2} = 2$ and $\bar{c}_k = 1$ for $1 \le k \le N/2 - 1$. Like other direct methods, pseudospectral methods can be sensitive to the initial guess and the nonlinear programming (NLP) solver used. Yan et al.[13] discuss these ideas in detail, and the method of generation of the initial guess by integration of the equations of motion for a given control set is used with NPSOL[14] as the NLP solver. This has been found to be quite satisfactory for the problem studied in this Note.

The original problem is converted into an NLP problem by enforcement of the state equations as equality constraints at the CGL nodes and the use of the values of the states and controls at the CGL nodes, the tether cross-sectional area, and the final time as optimization parameters. Further details of the solution method are given in Ref. 11. The resulting NLP problem is solved with NPSOL,[14] which is written in FORTRAN and called from MATLAB® via mex file interfaces. The Jacobian of the constraints, as well as the gradient of the performance index, are provided analytically, except for the derivatives of the eccentricity constraint, which are approximated by the use of finite differences due to their complexity.

Numerical Results

The optimal control problem is solved for a variety of cases by the use of $N = 50$. This was selected based on convergence of the cost function to within 1%. A set of common initial conditions is used for all computations, $\{\theta_0, \theta_0', \Lambda_0, \Lambda_0'\} = \{\pi, 0, 1, 0\}$. The initial conditions represent that the payload is initially pointing toward the central planet with the tether aligned along the local vertical, nonspinning, and deployed at the reference length. This is intuitively more practical than the requirement that the tether to be in an initially spinning configuration. The initial true anomaly t_0 is set as

$$t_0 = \pi/6 - \cos^{-1}(1/e) \tag{21}$$

which is selected to ensure that the tether system is within the target planet's sphere of influence. The initial guess for the nonlinear

solver is generated by integration of the tether system equations of motion for a fixed length tether with the initial conditions given earlier. Default tolerances are used in NPSOL, and, for validation purposes, the solution is propagated with the interpolated controls using MATLAB's ode45 routine with absolute and relative error tolerances set to 10^{-9}.

Optimal trajectories are determined at Venus and Jupiter for a range of values of the ratio of m_1/m_2. Nominally, $m_1 = 8000$ kg, which includes the tether mass.[4] The parameters used for the interplanetary arrival conditions are taken from Ref. 4 and are repeated in Table 1. The characteristics of the tether material are $\sigma_{ut} = 4$ GPa, $\rho = 970$ kg/m^3, $F = 1.5$, whereas the propulsion system assumes $I_{sp} = 300$ s as in Refs. 2 and 4. A summary of the maximum length rate, the ratio of tether mass to propellant mass, and the change in eccentricity from the case where the tether length is held fixed is given in Fig. 3. Example results of the optimal trajectory for the case of $m_1/m_2 = 10$ are presented in Figs. 4 and 5.

Table 1 Arrival conditions for the hyperbolic trajectory

Planet	μ, km^3/s^2	v_∞, km/s	r_p, km	e	Δv, km/s	L, km
Venus	3.25×10^5	2.71	6,550	1.148	0.362	150
Jupiter	1.27×10^8	5.64	72,300	1.018	0.268	190

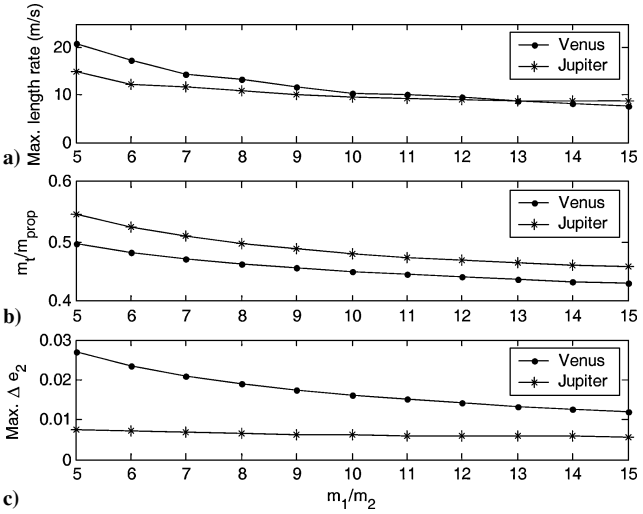

Fig. 3 Optimum results for controlled planetary capture: a) maximum length rate, b) ratio of tether mass to propellant mass, and c) maximum change in eccentricity from uncontrolled case.

Figure 3a shows that length rates of the order of 10–20 m/s are needed to control the planetary capture maneuver successfully. As the ratio of m_1/m_2 increases, both the maximum length rate and required tether mass decrease. This is reasonable because, as the payload mass decreases, the tether tension decreases; hence, less material is required. The required tether mass varies between 43 and 55% of the corresponding propellant mass. In addition, as m_1/m_2 increases for a given tether length, the payload's distance from the center of mass increases, resulting in a larger Δv at the tether tip for the same angular velocity. Therefore, less intervention from tether reeling is required. This is consistent with Fig. 3c, which shows that the required change in eccentricity due to tether reeling decreases as m_1/m_2 increases. The results for the required tether mass are even more impressive when it is considered that there is a factor of safety of 1.5 on the tether material and that the controlled tether maneuver causes the payload to enter into a 0.995 eccentricity elliptical orbit, whereas the propellant maneuver is based on a hyperbolic to parabolic orbit transition. Note that it is advantageous to make this ratio as large as possible to reduce both the tether mass and maximum required length rate. The consequence of this, however, is that the boost in velocity of the main spacecraft is reduced (not shown).

Example optimal trajectories are given in Figs. 4 and 5, which are typical for different values of m_1/m_2. Figures 4a and 5a show that intervention of the control system is implemented before periapsis. This occurs because of the low tension in the tether during this stage of the hyperbolic orbit (Figs. 4d and 5d) and, therefore, results in less work being done by the reel system. At both Venus and Jupiter, the tether is required to be reeled out only. The reason for reeling the tether out is to increase the tether length and, hence, the Δv at the tether tip. In Ref. 4, maximum reel rates of approximately 150 m/s were reported for the Venus capture case ($m_1/m_2 = 10$), where a cost function involving the maximum reel rate and penalty functions for the constraints was used. It is evident from the results obtained in this Note that much more efficient maneuvers are possible.

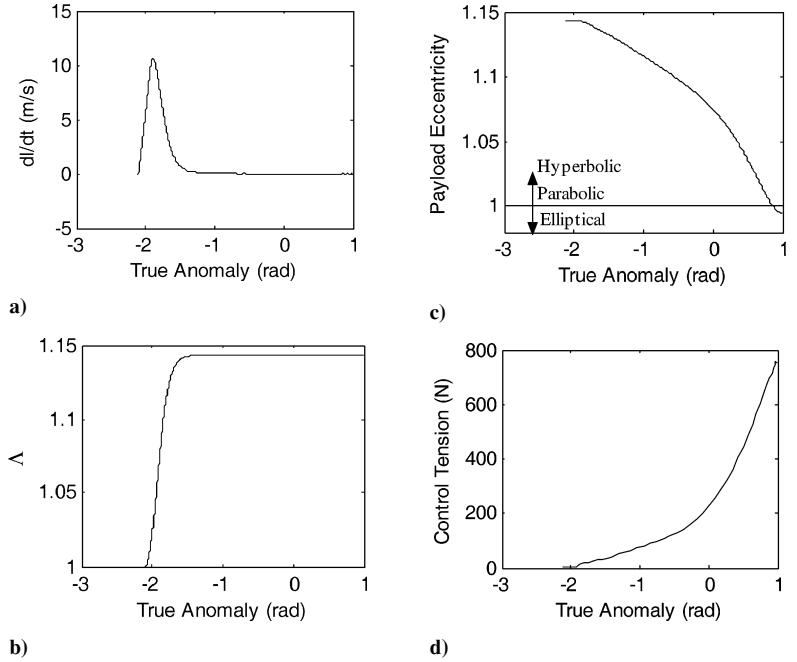

Fig. 4 Optimum results for tethered planetary capture at Venus ($m_1/m_2 = 10$).

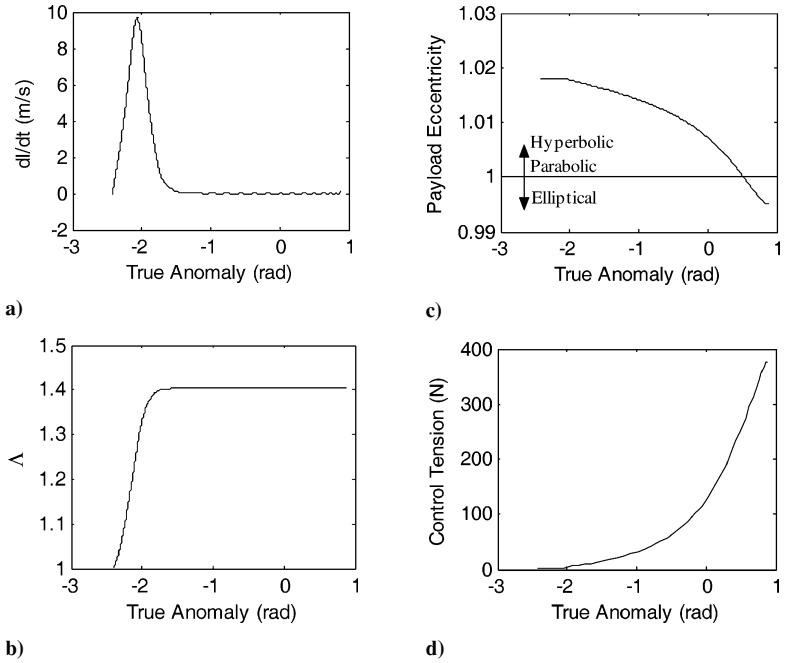

Fig. 5 Optimum results for tethered planetary capture at Jupiter ($m_1/m_2 = 10$).

Conclusions

A Chebyshev pseudospectral method has been used to obtain optimal trajectories for tethered planetary capture missions. Maximum tether reel rates and tether mass are calculated for mass ratios between 5 and 15 of the main spacecraft mass to payload mass. Numerical results show that it possible to transfer a payload from a hyperbolic orbit to an elliptical orbit by the use of practical tether reel rates (10–20 m/s) at both Venus and Jupiter. The tether mass required to sustain the tension forces is between 43 and 55% of the propellant mass needed to perform a similar maneuver using rocket propulsion. It is apparent that tethers provide an efficient means for performing controlled planetary capture maneuvers and may be an important tool for future space exploration.

References

[1]Beletsky, V. V., and Levin, E. M., "Dynamics of Space Tether Systems," *Advances in the Astronautical Sciences*, Vol. 83, 1993, Chap. 1.

[2]Longuski, J. M., Puig-Suari, J., and Mechalas, J., "Aerobraking Tethers for the Exploration of the Solar System," *Acta Astronautica*, Vol. 35, No. 2–3, 1995, pp. 205–214.

[3]Williams, P., Blanksby, C., and Trivailo, P., "Tethered Planetary Capture: Controlled Maneuvers," *Acta Astronautica*, Vol. 52, No. 4–10, 2003, pp. 681–708.

[4]Williams, P., Blanksby, C., and Trivailo, P., "Tethered Planetary Capture Maneuvers," *Journal of Spacecraft and Rockets* (to be published).

[5]Arnold, D. A., "The Behavior of Long Tethers in Space," *Journal of the Astronautical Sciences*, Vol. 35, No. 1, 1987, pp. 3–18.

[6]Kirk, D. E., *Optimal Control Theory: An Introduction*, Prentice–Hall, Upper Saddle River, NJ, 1970, Chap. 6.

[7]Ohtsuka, T., and Fujii, H., "Stabilized Continuation Method for Solving Optimal Control Problems," *Journal of Guidance, Control, and Dynamics*, Vol. 17, No. 5, 1994, pp. 950–957.

[8]Betts, J. T., "Survey of Numerical Methods for Trajectory Optimization," *Journal of Guidance, Control, and Dynamics*, Vol. 21, No. 2, 1998, pp. 193–207.

[9]Hull, D. G., "Conversion of Optimal Control Problems into Parameter Optimization Problems," *Journal of Guidance, Control, and Dynamics*, Vol. 20, No. 1, 1997, pp. 57–60.

[10]Ross, I. M., and Fahroo, F., "Legendre Pseudospectral Approximations for Optimal Control Problem," *Lecture Notes in Control and Information Sciences*, Springer-Verlag (to be published).

[11]Fahroo, F., and Ross, I. M., "Direct Trajectory Optimization by a Chebyshev Pseudospectral Method," *Journal of Guidance, Control, and Dynamics*, Vol. 25, No. 1, 2002, pp. 160–166.

[12]Melton, R. G., "Comparison of Direct Optimization Methods Applied to Solar Sail Problems," AIAA Paper 2002-4728, Aug. 2002.

[13]Yan, H., Fahroo, F., and Ross, I. M., "Accuracy and Optimality of Direct Transcription Methods," *Advances in the Astronautical Sciences*, Vol. 105, 2000, pp. 1613–1630.

[14]Gill, P. E., Murray, W., Saunders, M. A., and Wright, M. A., "User's Guide to NPSOL 5.0: A Fortran Package for Nonlinear Programming," Stanford Optimization Lab., TR SOL 86-1, Stanford Univ., Stanford, CA, July 1998.

C. Kluever
Associate Editor